A&A 400, 421–428 (2003)
DOI: 10.1051/0004-6361:20021716

Astronomy & Astrophysics

The nature of arms in spiral galaxies⋆

II. The sample

M. S. del Río[1] and J. Cepa[2,3]

[1] INAOE, 72000 Puebla, Mexico
[2] Instituto de Astrofísica de Canarias, 38200 La Laguna, Tenerife, Spain
[3] Departamento de Astrofísica, Facultad de Física, Universidad de La Laguna, 38071 La Laguna, Tenerife, Spain

Received 13 February 1998 / Accepted 7 October 2002

Abstract. We present here the results of an imaging study of eight grand-design and two intermediate-arm galaxies, based on CCD observations in U, B, V, R and I. We give grey-scale images, both in individual and in colour indices. Also we present a decomposition into bulge and disc following an iterative method. This provides us with a reasonable estimate of the bulge size and disc scale length, and shows the disc deviation from an exponential law, which can be interpreted as due to the long-term star formation caused by the spiral arms. To evaluate the contribution of the spiral arms to the disc luminosity distribution, with the aid of a mask we have decomposed each image into two parts: arms (which include bulge and nucleus, and eventually bars) and inter-arms (which include the outer disc).
In subsequent papers in this series (del Río & Cepa 1998, hereafter Paper III; del Río & Cepa 1999, hereafter Paper IV) the data presented here are used to analyse the spiral structure of the galaxies of the sample, using the methods of Beckman & Cepa (1990, hereafter Paper I) and the Fourier transform method to find the different symmetry degrees.

Key words. galaxies: spiral – galaxies: structure

1. Introduction

In this paper, the second of a series of four, we present detailed surface photometry in several filters of a set of galaxies based on CCD images obtained at the Isaac Newton Telescope (INT) and derive important basic photometric parameters of these galaxies: position angle and inclination from elliptical fits to external isophotes (assuming that they are circular), two-dimensional colour-index distributions and radial-luminosity profiles in each observed band, and, with these data, we perform a careful bulge–disc decomposition of the galaxies by taking into account the information provided by the colour indices in order to consider the effects of the young stellar population and dust, and to draw some general conclusions about the physical factors which contribute to radial profiles of spirals, and as well as to perform an analysis of the different methods used in the bulge–disc decomposition.

The objects are selected from a larger complete sample of field spiral galaxies that are close enough to resolve the spiral arms and with inclination less than 50° (except for NGC 6764). All but two are grand design (class 12 and 9 in the Elmegreen & Elmegreen 1987 classification). Galaxies belonging to class 12 have two long symmetric arms that dominate the optical disc. Galaxies belonging to class 9 (there are no classes 10 and 11) have two symmetric inner arms and multiple external long and continuous arms. Finally, we study, for comparison, two class 5 galaxies, which are characterized by two short symmetric inner arms, and several outer irregular arms. These galaxies were selected in order to study the spiral structure and the influence of density waves on star formation by analysing azimuthal profiles and bi-dimensional Fourier transforms. The results are described in Papers III and IV, respectively.

After calculating luminosity profiles we average the values for a constant radius by performing the bulge–disc decomposition, first for all the disc and later by distinguishing between the arm and the disc contributions. While the colour-index distribution does not vary so much between arms and inter-arms, the luminosity profiles show differences when removing the arms from the global image.

This paper presents the details of the observations and the reduced photometric profiles for the ten galaxies. In Sect. 2 the details of the observations and data reduction methods are discussed. In Sect. 3 colour and colour-index maps are shown (and possible errors in the data are discussed). Section 4 presents the actual mean photometric radial profiles. In Sect. 5

Send offprint requests to: M. S. del Río,
e-mail: sole@inaoep.mx

⋆ Figures 1 to 4 and Fig. 7 are only available in electronic form at http://www.edpsciences.org

the bulge–disc decomposition is performed. In Sect. 6 the inclination and position angles are derived. A brief discussion is given in Sect. 7.

2. Observations and data reduction

The observations were taken on 1990 August 16–23, at the prime focus of the 2.5 m INT at the Observatorio del Roque de los Muchachos on La Palma (Spain). A GEC CCD chip was used as a detector, with a conversion factor from ADU to electrons ∼1. The photosensitive part of the chip (390 × 590 pixel, with 10 columns of overscan excluded) represents an area of the sky of 3.5′ × 5.3′, i.e. a scale of 0.54″ per pixel. During the observations the seeing remained constant at around 1–1.3 arcsec. The nights were very clear, without dust, clouds or wind, and the relative humidity was low.

The photometric bandpass filters used were the Kitt Peak broadband (Kron–Cousins system) *U*, *B*, *V*, *R* and *I*, with typical exposure times of 1800 s, 1200 s, 600 s, 300 s and 300 s respectively. With these exposure times we can resolve the arms clearly, although in some cases (mainly the *R* and *I* bandpasses) the nucleus is saturated; but saturation affects only a few central pixels, never the spiral arms. The spectral filter response convolved with the GEC detector can be found in Benn & Cooper (1987).

The observations were reduced in a standard way: bias correction (up to ten were taken each night), sky flat-field normalization, and sky subtraction. No dark count correction was applied since this was significantly lower than the readout noise for the integration times employed. Images were processed using the FIGARO package and our own software.

All the frames of a given galaxy in different bands were re-centred by fitting field-star profiles. This allows precise colour images to be obtained. Images were re-centred with an accuracy of several thousandths of a pixel in most of cases, and a tenth of a pixel in the two worst cases (the *y*-axis in the *U* band of NGC 6951 and NGC 895), to avoid colour gradients caused by misalignment of the images. The field stars for re-centring were selected very carefully, because, while in the *U* band the star could have enough S/N, the *I* band could well be saturated. Finally between five and seven non-aligned stars were selected by frame in every band and galaxy. A subsequent check of the goodness of our method is the spatial agreement of maxima of field stars in the azimuthal profiles in the different bands.

The images were flux-calibrated by auxiliary observations of the standard star FZ 24 from the Landolt (1983) catalogue, using the same configuration of the instrumentation and similar reduction procedures, using double (star and sky) aperture photometry.

3. Colour and colour-index maps

In Figs. 7a–j we present the basic reduced data set for all the galaxies. These consist of an image of each object in each band, calibrated in mag arcsec^{-2}, and its corresponding isophotal map together with one colour-index image (*B*–*I*) for each object.

The colour-index images, in Fig. 7, convey two types of information whose combination can make interpretation quite complex. Where the image is red (darker shades) we can infer either that the population is older or more metallic than in the bluer areas (lighter shades), or that we are observing starlight partly obscured by dust. Qualitatively, it is often possible to distinguish which of these two cases predominates. From the present set of galaxies, NGC 157 and NGC 895 have well-defined red features which show up sharply in *B*–*I*, and coincide spatially with reduced intensity in the single band images, notably in *U* and *B*. This coincidence, and the characteristic patchy appearance of the redder zones, leads to the conclusion that we are observing reddening due to dust extinction.

In NGC 6384 and NGC 7479 we also see obvious dust reddening where the darker zones in *B*–*I* coincide with reduced *B* intensity, but in these galaxies there is also a tendency towards increased redness towards the centre of the bulge which coincides with enhanced intensity, even in the *B* band. This trend is probably attributable to population contrast, with older stars towards the nuclei of these galaxies.

NGC 6814 and NGC 6951 are mixed cases where both phenomena are present.

The colour index maps show a pronounced uniformity. The arms, clearly distinguishable in every broad band, are not much bluer than inter-arm regions, only sharply defined zones with intensive star formation being notably conspicuous. We have not detected any relevant colour gradient in the arms.

A possible error in subtraction of the sky in the original images is one of the biggest sources of error in their calibration and mainly affects those zones where the number of counts per pixel is low (magnitudes higher than 21 μ). In the radial profiles, (described in Sect. 4) we performed a test to check how these vary when the sky is underestimated by one, two, three or four counts, and also when the sky is overestimated by similar amounts. In the former case we subtracted from the original frame, calibrated in flux, the counts mentioned above. We recalibrated the image and recalculated the radial profiles. In all cases the noise rises noticeably, and in the redder bands we observe a progressive change of the scale length. In the bluer bands the noise is so high that the behaviour of the scale length becomes erratic. In the case where the sky has been overestimated, we added counts to the flux image, and we again proceeded to recalibrate the image and recalculate the radial profiles. In this case the noise did not increase, but the scale length did, and in a spectacular manner. In fact, with a difference of only one count, the profiles in the *B* band changed from 25 μ to only 22 μ, for the same radius. Differences proportional to those in *B* are found in the other bands. These tests led us to believe that the sky background, as determined in the original calibration of the data, is indeed reliable.

The radial profiles, shown in Figs. 1–3, do not terminate in either a very noisy zone or in very low magnitudes (see Table 1). This confirms that the calibration of the galaxies is correct.

4. Mean radial profiles

The radial profiles were derived from the azimuthal ones (see Paper III). First, from each original image we removed the brightest stars in the inter-arm and outer regions. To do this

Table 1. Lower and upper magnitude for each object.

Object	*U*		*B*		*V*		*R*		*I*		*B* − *I*	
	min	max	min	max	min	max	min	max	min	max	min	max
NGC 0157	19.4	24.6	18.9	25.8	18.0	25.2	17.8	24.9	17.1	24.1	0.22	3.97
NGC 0753	20.0	23.5	19.2	24.5	17.9	23.9	17.4	23.3	16.5	22.3	0.31	4.92
NGC 0895	20.3	23.3	19.9	25.6	19.2	25.1	18.5	24.4	18.0	23.7	−1.00	3.96
NCG 4321	19.1	26.8	18.3	25.0	18.0	25.5	18.5	26.0	17.9	25.2	0.42	4.27
NGC 6384	19.4	24.6	18.7	25.3	17.5	24.7	17.7	24.5	17.2	23.2	−0.39	3.75
NGC 6764	17.3	24.5	19.4	25.0	17.9	23.8	17.8	23.1	17.2	22.1	1.19	4.18
NGC 6814	17.1	24.9	18.0	25.5	17.1	24.5	17.8	24.1	17.2	23.4	−0.75	3.35
NGC 6951	19.3	25.0	18.9	25.7	17.7	24.9	17.7	24.5	17.1	23.5	−0.69	3.64
NGC 7479	19.7	24.0	19.2	24.7	18.2	24.1	17.7	23.9	16.9	22.9	1.77	4.23
NGC 7723	17.6	24.3	18.1	25.8	17.8	25.1	17.8	24.8	17.2	23.8	0.17	3.38

we take a square over the area occupied by the star, and replace the pixel values with the mean value of nearby pixels. While in azimuthal-profile analysis field stars cause little disturbance and are relatively easy to avoid during the analyses (see Paper III), Fourier transform decomposition is seriously affected by the presence of these stars, which cannot be removed or avoided after decomposition (see Paper IV). Secondly, we take 288 azimuthal profiles (from 1 pixel radius to the end of the frame), in steps of 0.54″ (our physical resolution before smoothing the data). Finally, for each radius we calculate the average flux value, excluding points with values lower than 0.005 count s^{-1} (lower than ≈26 μ in the *U* band and ≈28 μ in the *I* band, where μ is mag arcsec^{-2}).

The main advantage of this method over procedures based on isophotal contours weighted with the major-axis flux is that no arbitrary direction is privileged over any other and results are radius-dependent, not fitting-dependent, and can then be easily compared with other data. However, this method can smears non-axisymmetric features, mainly the spiral arms or bars, but this problem can be solved by decomposing each image in arm and inter-arm images, and then applying this method to calculate radial profiles separately. Anyway, the smoothing provoked by averaging the global image is not so serious, as we can confirm by the effect of field stars of medium brightness.

Where possible, we separated the arms from the global image, and re-calculated the mean radial profile for arms and for inter-arms. In Fig. 1 we show radial profiles in each band (continuous line). Dotted lines correspond to inter-arm regions (which include external disc) and dashed lines correspond to arms (which include bulges and/or bars). As we can see in Fig. 1 arms are much brighter than inter-arms, especially in bluer bands, and have smoother slope (i.e. a large scale length), but their contribution to the total brightness is not very important (see Fig. 4). The arms of spiral galaxies fill a small fraction of the whole disc, mainly in the outer regions (see Fig. 4). Averaging the brightness at a fixed radial distance, arms are quickly dominated by inter-arm light. A similar general behaviour in every galaxy of the sample can be seen. While disc profiles (which include the inter-arm zone) are almost identical to global profiles, arm brightness profiles are absolutely different in that they are much more "flat" and brilliant. The percentage of light that arms contribute to the global brightness profile in each band and galaxy can be seen in Fig. 1. In this figure we can find features that are no obvious to the eye. NGC 157 has two long and symmetric bright arms, but which contribute (except in two small ranges, even in the *U* band) rather less than 50% to the global profile, while in the case NGC 6951, the arms, which are weak, represent more that 50% of global profile even beyond the end of the bar (which occurs at ∼50″).

When arms are eliminated from the flux image and radial profiles are calculated, we can see that the change in the slope, when present, persists (see Fig. 1). This means that the arms are not directly responsible for a such change in the slope, although it matches with the end of them. One possible explanation would be that the arms, and the innermost part of the disc, have a radial exponential distribution, with a scale length much longer than that of the outer disc. The end of the disc would match with the end of the arms, and from this point, the decrease in brightness would be exponential until reaching the underlying disc. This may explain such cases as that of NGC 157, where, fitting an exponential profile to the outer disc ($R > 60''$), we obtain a central brightness higher than that of the bulge, so the decomposition into a disc (exponential) and a bulge (exponential or de Vaucouleurs) is unfeasible from the outset. In galaxies where the change in the slope is not so abrupt, such as NGC 895, it is possible to decompose the profile as the sum of two functions, but then the zone of the arms is overestimated in the fit.

5. Bulge-disc decompositions

The major conceptual problem inherent to all methods of separating luminosity profiles into disc and bulge contribution is that one must assume the fitting functions. We have chosen the de Vaucouleurs law for bulges (Eq. (1)) and an exponential law for discs (Eq. (2)):

$$\mu_{\rm bulge} = \mu_{\rm b} + 8.325\left[(r/r_{\rm b})^{1/4} - 1\right] \quad (1)$$

$$\mu_{\rm disc} = \mu_{\rm d} + 1.082(r/r_{\rm d}). \quad (2)$$

In these equations μ is the surface brightness in mag arcsec^{-2} at a radius r; $\mu_{\rm b}$ and $\mu_{\rm d}$ are characteristic surface brightnesses;

r_d is the effective radius containing one-half the total light of the disc, and r_b is the bulge scale length.

The method followed in decomposing our profiles is Kormendy's (1977) iterative procedure. First, two ranges of radii are chosen, one where the disc clearly dominates the profile and one in which the bulge contribution is more important. Then the disc fitting function is fitted by least squares to the data within the disc-dominated fitting range. This calculated disc contribution is then subtracted from the observed data points at all radii, and these corrected data are fitted to the bulge fitting function in the range dominated by bulge light. This fit is then subtracted from the original observed profile, and then the process is repeated until it converges, usually after no more than ten iterations. In Fig. 2 we show the best fit to each filter for each galaxy.

This kind of decomposition (de Vaucouleurs bulge + exponential disc) is purely empirical, the laws used are strictly empirical fitting functions. Such profile decomposition is, without doubt, the most usual, but is not the only one. Some authors prefer not introduce any pre-set analytic function, but use iterative fits instead (Kormendy 1977), while others fit more than one exponential (usually two) to galaxies with light profiles similar to those of NGC 157 or NGC 895 in Fig. 2 (two non-barred galaxies that show a "step" in their profiles).

Some galaxies cannot be fitted by these simple functions; for example, Freeman's 1970 type II discs, or galaxies with strong bars. In two cases the iterative method clearly diverges: in the U band of NGC 753 (due probably to the low signal-to-noise ratio) and in the R band of NGC 6764, a barred galaxy with faint arms. In other cases we cannot produce a sum of these two functions to fit the observed profiles. That is the case for NGC 157 and NGC 895, two non-barred galaxies, where the disc fit must be done in the inner part where the arms exist (until $R \sim 65-70''$ for the first and $R \sim 60''$ for the second), because if the fit is made over the outer disc, the extrapolation as far as the nucleus leads to a luminosity higher than that observed. For these particular cases we have eliminated the arms with several kinds of masks, both including and excluding the bulge. However, the general shape of the profile hardly changes. Therefore we can conclude that, although the presence of the bars or spiral arms distorts the luminosity radial profiles, causing departures from the assumed exponential form, there should be another effect that explains this feature. Indeed it seems that there is a lack of light in the central zones of several galaxies in the sample, compared with what we might expect for an exponential distribution. There could be several reasons for this; for example, galactic discs could decompose into more than one exponential, or the fitting functions might actually more complex. Another possibility is that the inner part is obscured by dust. This could explain why, in some cases, an exponential light distribution correctly fits the observed radial profiles (in what would presumably be dust-poor galaxies), whereas it does not fit in others (in what would presumably be dust-rich galaxies). Under this hypothesis, the slope changes are located at the end of spiral arms, where star formation is more intense, and the amount of dust is therefore a priori higher.

The iterative bulge–disc decomposition works well in four of the ten galaxies of the sample (NGC 4321, NGC 6384, NGC 6814 and NGC 7723), but does not work in any band for NGC 6764 (a class 5 galaxy, much more faint than the others of the sample) and throws up different problems in the remaining cases. Galaxies with a prominent bar, such as NGC 6951 and NGC 7479, cannot be decomposed with this method if we do not take into account the contribution to the profile of the light from the bar. Galaxies with fainter bars, such as NGC 4321, do not present this problem. Nevertheless, it is not only the bars that produce severe discrepancies between the light profile and the sum of an exponential and a de Vaucouleurs component. This is the case of NGC 157 and NGC 895, the two grand design non-barred galaxies already mentioned. The resulting profiles, with and without masks, are shown in Fig. 1.

Three groups can be formed with the goodness-of-fit selection criterion:
a) Good fits: NGC 4321, NGC 6384, NGC 6814;
b) Poor fits: NGC 157, NGC 895, NGC 6764, NGC 7479;
c) Intermediate fits: NGC 753, NGC 6951, NGC 7723.
NGC 6951 is a somewhat special case. In the U band the exponential fit to the disc is very good until the sky level ($\sim 25\ \mu \approx R \sim 110''$) is reached: we cannot distinguish the bar and dust effects are not very conspicuous. Nevertheless, in the I band the agreement is worse from $R \sim 100''$, a value that roughly matches the end of the faint outer arms ($\sim 22.5\ \mu$). This can be explained as a population effect. Recent star formation is rare in this galaxy, so in the U band (and possibly in B too), the galaxy can be divided into a not very extended bulge ($r_b \sim 0.1-0.3$ kpc) and a smooth disc ($r_d \sim 5$ kpc). The old population, however, is re-organized by a relatively strong, but low-efficiency, spiral density wave (Paper III), which reaches a radius of $\sim 100''$ (~ 9.2 kpc, less than two scale lengths), and the flux is no longer uniformly radially distributed in the redder bands.

As we mentioned before, the exponential disc + de Vaucouleurs bulge is the most popular decomposition, but by no means the only one. Several authors (Frankston & Schild 1976; Kent et al. 1991; Andredakis & Sanders 1994) have proposed an exponential fitting function for the bulge also:

$$\mu_{\rm bulge} = \mu_{0b} \cdot e^{-r/r_b}, \tag{3}$$

where r_b is the scale length of the bulge. In fact, the use of an exponential bulge improves the quality of the fits (Fig. 3), even though some problems still remain. Profiles such as those of NGC 6764, and perhaps part of the profile of NGC 895, could be better fitted by adding as proposed by Serna (1997), an arm contribution as a sinusoidal distortion of an exponential disc; however, this method also fails to explain the change in slope in the other galaxies. This change is located very close to the end of the arms in the four cases, but the slope decreases with respect to the slope of the former part. If we add the arm contribution we would expect a relative increase in the slope. Undoubtedly, this change is closely related to the spatial extent of the arms, because when arms are removed, the change persists. This contradiction, however, is more apparent than real. The arms do not cause the change in the slope, but coincide

Table 2. Bulge scale-length, in kpc, calculated from decomposition bulge-disc. de Vaucouleurs law for bulge. Distances are calculated with $H_0 = 75\,\mathrm{km\,s^{-1}\,Mpc^{-1}}$.

NGC	157	753	895	4321	6384	6764	6814	6951	7479	7723
U	0.02	···	6.79	0.05	1.44	3.05	0.02	0.08	21.75	0.27
B	0.24	9.90	4.11	0.02	2.12	2.77	0.19	0.27	21.83	0.02
V	0.40	7.49	3.56	0.04	2.32	4.06	0.45	0.49	16.97	0.36
R	0.79	9.54	3.55	0.11	2.36	···	0.56	0.65	12.85	2.45
I	0.98	7.97	3.50	0.20	2.75	3.04	0.77	1.05	11.33	4.96

Table 3. Disc scale-length, in kpc, calculated from decomposition bulge-disc. de Vaucouleurs law for bulge.

NGC	157	753	895	4321	6384	6764	6814	6951	7479	7723
U	9.36	···	14.36	6.37	8.74	4.22	3.60	5.56	36.49	3.10
B	7.86	6.80	10.79	8.08	7.71	3.59	2.68	4.25	21.32	2.70
V	6.57	6.40	8.69	6.68	7.24	3.18	2.56	4.00	14.21	2.71
R	6.52	6.49	8.29	6.72	6.89	···	2.51	4.14	11.88	2.68
I	5.85	4.91	7.47	6.82	6.65	3.10	2.47	4.30	9.58	2.46

Table 4. Bulge scale-length, in kpc, calculated from decomposition bulge-disc. Exponential law for bulge.

NGC	157	753	895	4321	6384	6764	6814	6951	7479	7723
U	0.09	1.47	0.80	0.28	0.50	1.37	0.10	0.21	0.94	0.46
B	0.16	0.98	0.79	0.22	0.54	1.50	0.19	0.28	0.93	0.08
V	0.18	0.93	0.78	0.27	0.55	1.42	0.23	0.32	0.89	0.17
R	0.20	0.98	0.78	0.35	0.55	1.72	0.25	0.34	0.85	0.26
I	0.21	0.97	0.78	0.40	0.56	1.03	0.26	0.37	0.82	0.31

Table 5. Disc scale-length, in kpc, calculated from decomposition bulge-disc. Exponential law for bulge.

NGC	157	753	895	4321	6384	6764	6814	6951	7479	7723
U	9.35	52.63	9.38	6.37	8.39	4.44	3.60	5.52	16.43	3.09
B	7.55	7.29	8.01	8.08	7.11	3.88	2.67	4.11	11.38	2.70
V	6.09	6.87	6.71	6.67	6.53	3.52	2.54	3.77	9.20	2.71
R	5.72	7.45	6.34	6.71	6.22	3.14	2.49	3.78	8.58	2.68
I	5.03	7.19	5.77	6.78	5.89	3.44	2.45	3.73	7.48	2.67

Table 6. Bulge scale-length, in kpc, calculated with only one fit.

NGC	157	753	895	4321	6384	6764	6814	6951	7479	7723
U	9.71	50.97	56.40	0.71	5.95	0.61	2.70	0.45	37.27	5.75
B	3.73	23.45	33.84	0.20	5.10	1.08	4.00	1.00	31.80	8.39
V	2.98	14.69	22.99	0.40	4.57	1.70	4.20	1.45	23.88	9.12
R	4.80	12.82	19.48	1.11	4.45	3.40	4.50	1.64	19.01	7.79
I	4.59	11.25	16.70	1.52	4.89	3.55	4.90	2.37	16.28	6.71

with the steepest slope. In fact, as can be see in Fig. 1, the arms smooth out the difference.

Once a sinusoidal arm contribution is discarded as the cause of this feature, the question remains as to what could be the mechanism (or mechanisms) that give rise to the change in the slope, or, more specifically, what might be the mechanism that, being related to the well-defined spiral arms, could also be related with the change in the slope of the radial profiles. Spiral density waves are the answer.

Intermediate galaxies do not show this change. Its apparent existence in NGC 7723 is not real at all. The outer arms of this galaxy barely reach $R \sim 70''$ (the probable outer Lindblad resonance, Paper III), and the change occurs at $R \sim 100''$, rather far away to be related to the arms or even the disc (see Paper IV).

Table 7. Disc scale-length, in kpc, calculated with only one fit.

NGC	157	753	895	4321	6384	6764	6814	6951	7479	7723
U	9.28	55.03	7.03	6.90	8.61	4.48	4.80	4.74	8.82	3.00
B	7.47	6.56	4.39	9.23	6.91	3.86	2.90	3.28	5.78	2.63
V	5.97	6.25	4.24	7.20	6.27	3.40	2.70	3.10	4.10	2.63
R	5.65	7.19	4.24	7.51	5.95	3.09	2.50	2.91	4.10	2.63
I	4.91	6.87	4.10	7.41	5.53	3.40	2.50	2.91	6.08	2.63

Table 8. Data marked with † are from RC3, data marked with ‡ are from Grosbøl (1985). For NGC 4321 we have used $i = 31°$ and PA = 151°, from Cepa et al. (1992). Data marked with * have been calculated in this work. NGC 4321 and NGC 6384 are too large to properly calculate their D_{25}.

Object	PA†	$i^{\dagger}$	PA‡	$i^{\ddagger}$	PA*	i^{*}	D (Mpc)	$D^{\dagger}_{25}$	D^{*}_{25}
NGC 0157	40°	50° ± 2°	35	45° ± 3°	45°	50°	22.24	1.62 ± 0.2	1.62 ± 0.03
NGC 0753	125°	39° ± 3°	112° ± 1°	46° ± 6°	126°	45°	65.15	1.40 ± 0.2	1.40 ± 0.05
NGC 0895	65°	45° ± 4°	116° ± 1°	50° ± 2°	114°	50°	30.52	1.56 ± 0.2	1.57 ± 0.02
NGC 4321	30°	32° ± 4°	58° ± 4°	25° ± 1°			21.15	1.87 ± 0.1	
NGC 6384	30°	49° ± 2°	31° ± 1°	50° ± 7°	33°	47°	22.17	1.79 ± 0.02	
NGC 6764	62°	56° ± 3°	62° ± 1°	62° ± 8°	59°	59°	32.21	1.36 ± 0.4	1.30 ± 0.05
NGC 6814		21° ± 21°	167° ± 23°	7° ± 1°	167°	7°	20.84	1.48 ± 0.2	1.50 ± 0.04
NGC 6951	170°	34° ± 5°	157° ± 4°	44° ± 1°	157°	44°	19.01	1.59 ± 0.2	1.56 ± 0.04
NGC 7479	25°	40° ± 3°	39° ± 1°	45° ± 4°	39°	45°	31.70	1.61 ± 0.2	1.60 ± 0.05
NGC 7723	35°	47° ± 3°	38° ± 1°	47° ± 1°	37°	48°	25.00	1.54 ± 0.3	1.50 ± 0.02

Table 9. Limit magnitude, in each band for all galaxies. ‡Because this galaxy occupies almost all the frame, these values are an approximation, with a maximum error estimated of 6% in *I* band.

NGC	$m_{G_{\lim}U}$	$m_{G_{\lim}B}$	$m_{G_{\lim}V}$	$m_{G_{\lim}R}$	$m_{G_{\lim}I}$
157	24.64 ± 0.49	25.80 ± 0.47	25.21 ± 0.45	24.96 ± 0.43	24.07 ± 0.42
753	23.49 ± 0.63	24.51 ± 0.59	23.89 ± 0.56	23.33 ± 0.55	22.32 ± 0.52
895	23.27 ± 0.43	25.58 ± 0.40	25.08 ± 0.45	24.41 ± 0.42	23.72 ± 0.42
4321‡	26.82	25.06	25.54	25.96	25.25
6384	24.64 ± 0.47	25.30 ± 0.52	24.67 ± 0.56	24.54 ± 0.48	23.19 ± 0.56
6764	24.47 ± 0.57	25.01 ± 0.51	23.85 ± 0.48	23.10 ± 0.45	22.12 ± 0.44
6814	24.94 ± 0.51	25.55 ± 0.40	24.54 ± 0.46	24.08 ± 0.41	23.42 ± 0.41
6951	25.05 ± 0.52	25.71 ± 0.47	24.86 ± 0.44	24.47 ± 0.42	23.50 ± 0.41
7479	23.97	24.72 ± 0.40	24.08	23.90	22.89
7723	24.34 ± 0.47	25.82 ± 0.47	25.09 ± 0.44	24.78 ± 0.43	23.83 ± 0.41

Two grand design galaxies, NGC 4321 and NGC 6384, cover the chip entirely, so we cannot compare them with the arm-free zone in the disc. Among the grand design galaxies, NGC 6814 and NGC 753 are two oddities. Their arms are very short, compared to the total disc, and multiple. If density waves are related with the change of the slope in the radial profiles, in these cases the waves are probably weak or not very coherent. In fact, NGC 6814 presents a dominant four-arm pattern (see Paper IV). Finally, four grand design galaxies in the sample have two long arms that terminate before reaching the edge of the chip and their images have sufficient signal to noise.

When arms are eliminated from the flux image and the radial profiles are calculated, the change in the slope, when present, persists (see Fig. 1). This means that the arms are not directly responsible for such change in the slope, although it matches with the end of them. One possible explanation would be that the arms, and the innermost part of the disc, have an exponential radial distribution with a scale length much longer than that of the outer disc. The outer edge of the disc would match with the ends of the arms, and from this point outwards, the decrease in brightness would be exponential, until reaching the underlying disc. This may explain cases such NGC 157, where, when fitting an exponential profile to the outer disc ($R > 60''$), we obtain a central brightness higher than that of the bulge, so the decomposition into a sum of a disc (exponential) and a bulge (exponential or de Vaucouleurs) is unfeasible from the start. In galaxies where the change in the slope is not so abrupt, such as NGC 895, it is possible to decompose the profile as the sum of two functions, but then the zone of the arms is overestimated in the fit.

The model of two discs plus a bulge is much more complex because the number of free parameters is double that in the

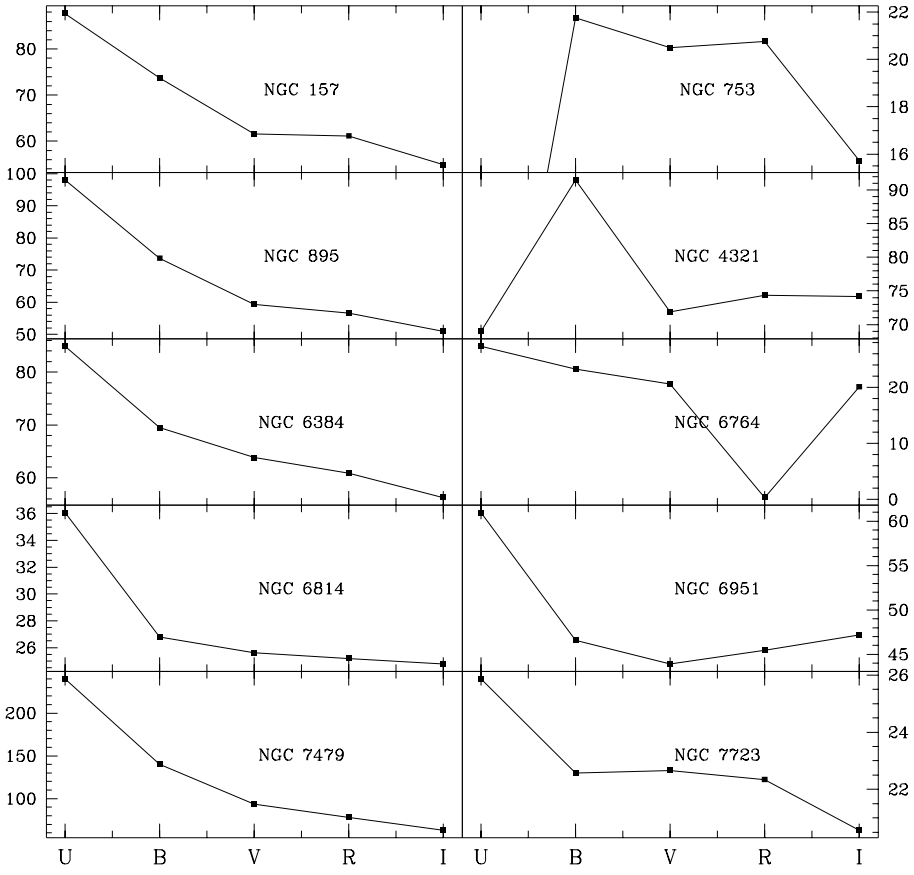

Fig. 5. Disc scale length as lengthwave function. dV law for bulge.

bulge + disc model (it is necessary to add the parameter of an underlying disc, the "arm" disc and the zone that connects both). So a qualitative parameterization could be arbitrary and subjective, even when the fit obtained is much better than that for the bulge+disc model.

6. Inclination and position angles

To derive the best pair of values for inclination and position angle (ω, PA), for each galaxy we fit an ellipse to the 25th μ contour in the B band, but only to points within a given distance from the ellipse; this is because external isophotes are quite irregular and "broad", so that there are points far away from the "elliptical" main body, with the same magnitude, that can not be excluded from the fit. With this technique we exclude possible contamination by external noise.

The procedure is as follows. From the 25 μ contour in the B band and a centre (calculated from non-saturated bands with the aid of field stars), for each pair of (ω, PA) values an ellipse is drawn over this contour. With a pre-set distance from the ellipse (usually 5″) we can calculate the quadratic distance:

$$d^2 = \sum (x_e - x_{25})^2 + (y_e - y_{25})^2, \quad (4)$$

where (x_e, y_e) are the points of the ellipse defined by (ω, PA), and (x_{25}, y_{25}) are the points of the 25th magnitude contour. So the minimum of d^2 should correspond to the best fit and the best (ω, PA) pair. But it could be the case that very few points lead to a small d^2 value, so the ellipse points used in Eq. (4) and the total number of ellipse points (due to the different values of inclination and size, the ellipses have different numbers of points) must be take into account. In fact we need to maximize a newly defined variable, η, equal to the product of the inverse of d^2 and the ratio of the isophote points used (UP) in the fit and the total number of points in the ellipse (TP):

$$\eta = \frac{1}{d^2} \cdot \frac{UP}{TP}. \quad (5)$$

We try various reasonable values of ω and PA, and use the pair that maximizes η.

The results are summarized in Table 8 and are in good agreement with values found by Grosbøl (1985) and de Vaucouleurs et al. (1991). We have not followed the other method usually used in calculating inclinations and position angles, the logarithmic fit to spiral arms, because, as will be demonstrated in Paper III, arms are not always logarithmic, can sometimes present a broken profile about midway from the centre and must be fitted with two logarithmic spirals.

7. Conclusions

The analytical decomposition of galaxies in bulge + disc components presents a series of unresolved problems. Usually, the de Vaucouleurs law gives bigger sizes for bulges than those calculated with the exponential law. Discs show similar scale

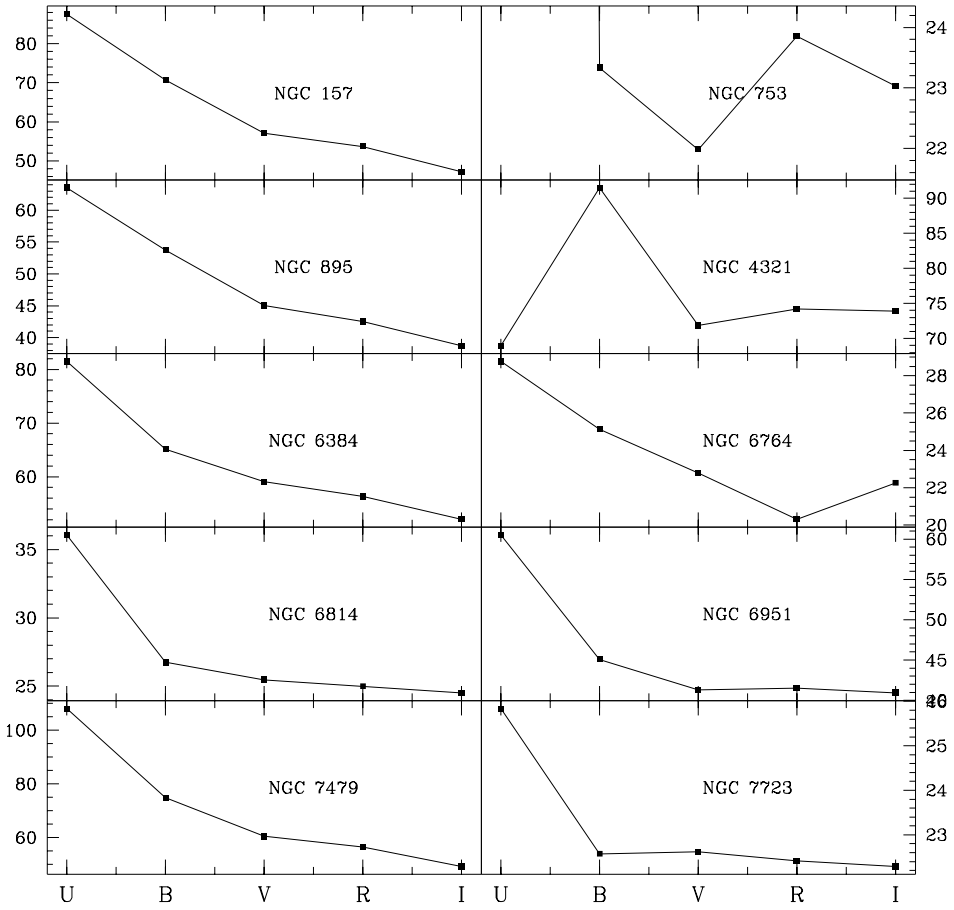

Fig. 6. Disc scale length as lengthwave function. Exponential law for bulge.

lengths with both decompositions, even when convergence is much faster with exponential bulges.

The contribution of the arms to the radial light profiles is not very significant. Although the arms have a scale length higher than inter-arm zones, the global profile of the galaxy does not vary so much when they are eliminated, probably due to their small filling factor.

External discs are well fitted by exponential functions, but when arms end before the disc terminates a change in the slope appears that cannot be fitted even if a sinusoidal contribution from the arms is taken into account. The presence of a bar does not significantly distort the profile, so the decomposition is not altered by it. In fact, the arms make a very small contribution to the luminosity profile for two main reasons: first because their filling factor is small, and secondly because they could be weak, as is the case of NGC 6951, with a relatively high filling factor, but whose arms are very weak.

Arms are not much bluer than inter-arm regions. *B–I* maps do not show prominent arms, even when colour images show very bright blue arms.

Acknowledgements. The Isaac Newton Telescope is operated on the island of La Palma by the Royal Greenwich Observatory in the Spanish Observatorio del Roque de Los Muchachos of the Instituto de Astrofísica de Canarias. This project was partially supported by the Spanish DGICYT grant No. PB94–0433 and the Mexican CONACyT grant No. 33026-E.

This research has made use of the NASA/IPAC Extragalactic Database (NED), which is operated by the Jet Propulsion Laboratory, California Institute of Technology, under contract with the National Aeronautics and Space Administration.

References

Andredakis, Y. C., & Sanders, R. H. 1994, MNRAS, 267, 283
Beckman, J. E., & Cepa, J. 1990, A&A, 229, 37 (Paper I)
Benn, C., & Cooper, D. 1987, RGO/La Palma Technical Note, 45
Cepa, J., Beckman, J. E., Knapen, J. H., Nakai, N., & Kuno, N. 1992, AJ, 103, 429
Elmegreen, D. M., & Elmegreen, B. G. 1987, ApJ, 314, 3
Frankston, M., & Schild, R. 1976, AJ, 81, 500
Freeman, K. 1970, ApJ, 160, 811
Grosbøl, P. J. 1985, A&AS, 60, 261
Kent, S. M., Dame, T. M., & Fazio, G. 1991, ApJ, 378, 131
Kormendy, J. 1977, ApJ, 217, 406
Landolt, A. U. 1983, AJ, 88, 853
del Río, M. S., & Cepa, J. 1998, A&A, 340, 1 (Paper III)
del Río, M. S., & Cepa, J. 1999, A&AS, 134, 333 (Paper IV)
Serna, A. 1997, A&A, 318, 741
de Vaucouleurs, G., de Vaucouleurs, A., Corwin, H. G., et al. 1991, Third Reference Catalogue of Bright Galaxies (New York, Springer)